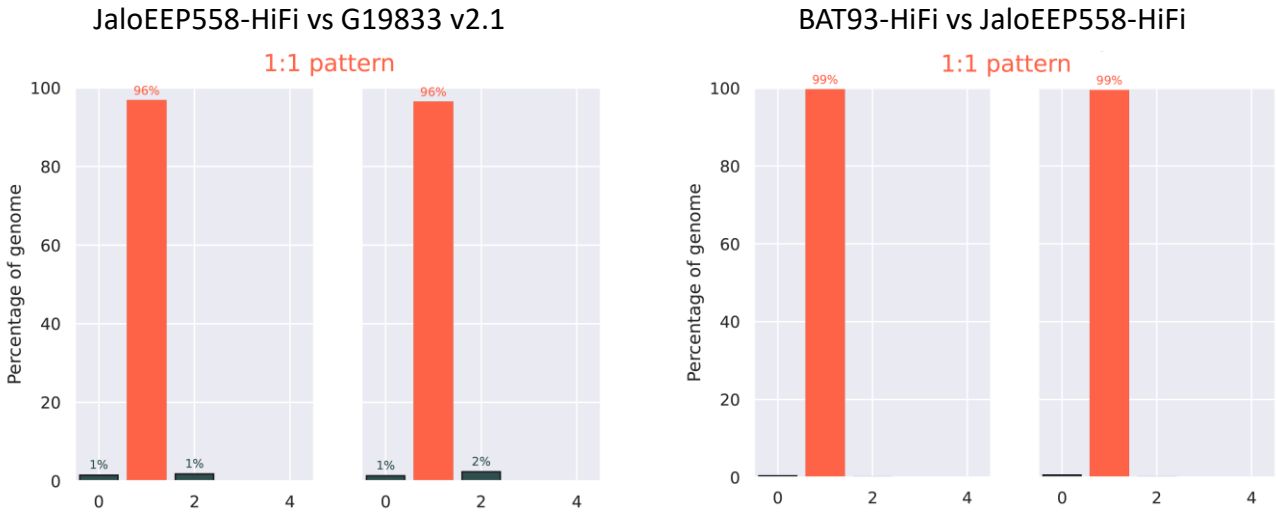

Supplementary Figure 1. Syntenic relationship between sequenced and reference genome assemblies

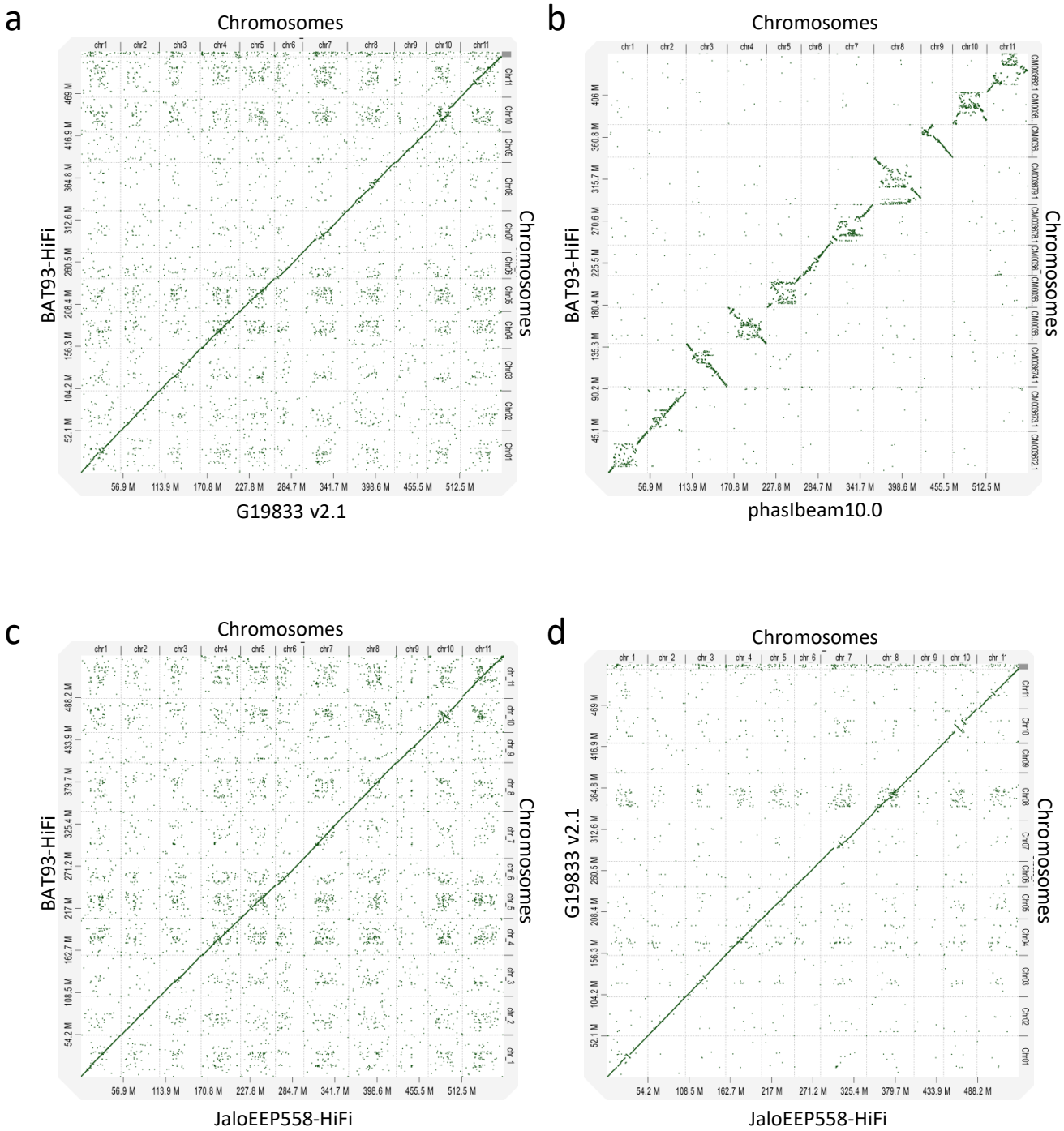

Supplementary Figure 2. Comparative synteny dot plot between assembled genomes of G19833 v2.1, BAT93-HiFi, JaloEEP558-HiFi and BAT93 (phasIbeam10.0)

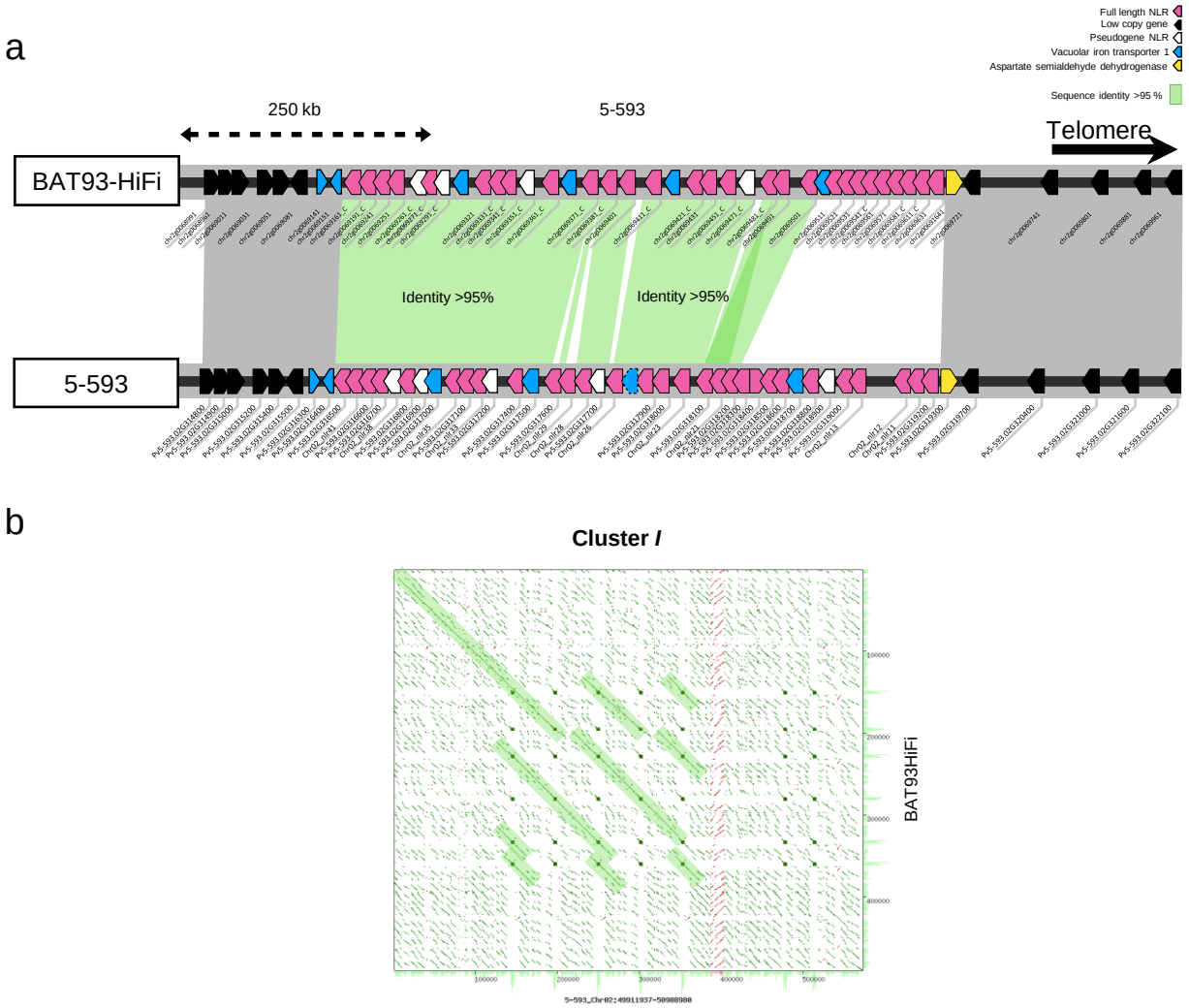

Supplementary Figure 3. Comparative analysis between two *I* bearing genotypes BAT93 and 5-593. a. Representation of the synteny of the *I* cluster. b. Dot-plot analysis of the *I* cluster between the two genotypes (TNL containing region).

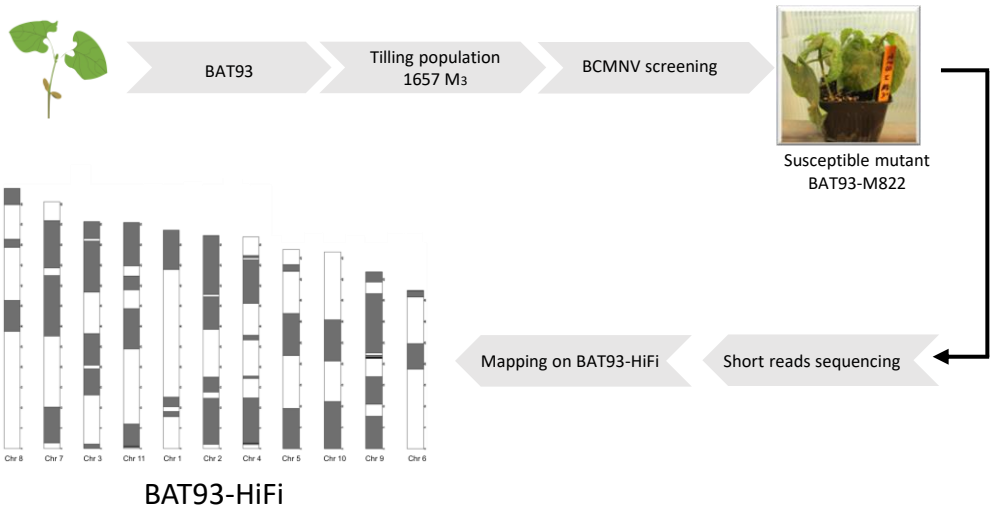

Supplementary Figure 4. Workflow for the identification of the *I* gene on the BAT93-HiFi genome assembly

I Gene (Chrg0069161)

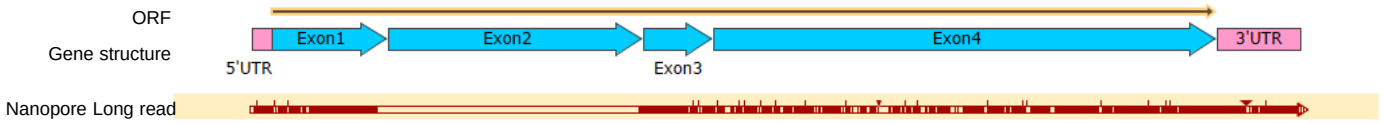

Supplementary Figure 5. Schematic representation of Nanopore long reads from BAT93-M822 mapped in the *I* gene showing exon 2 skipping

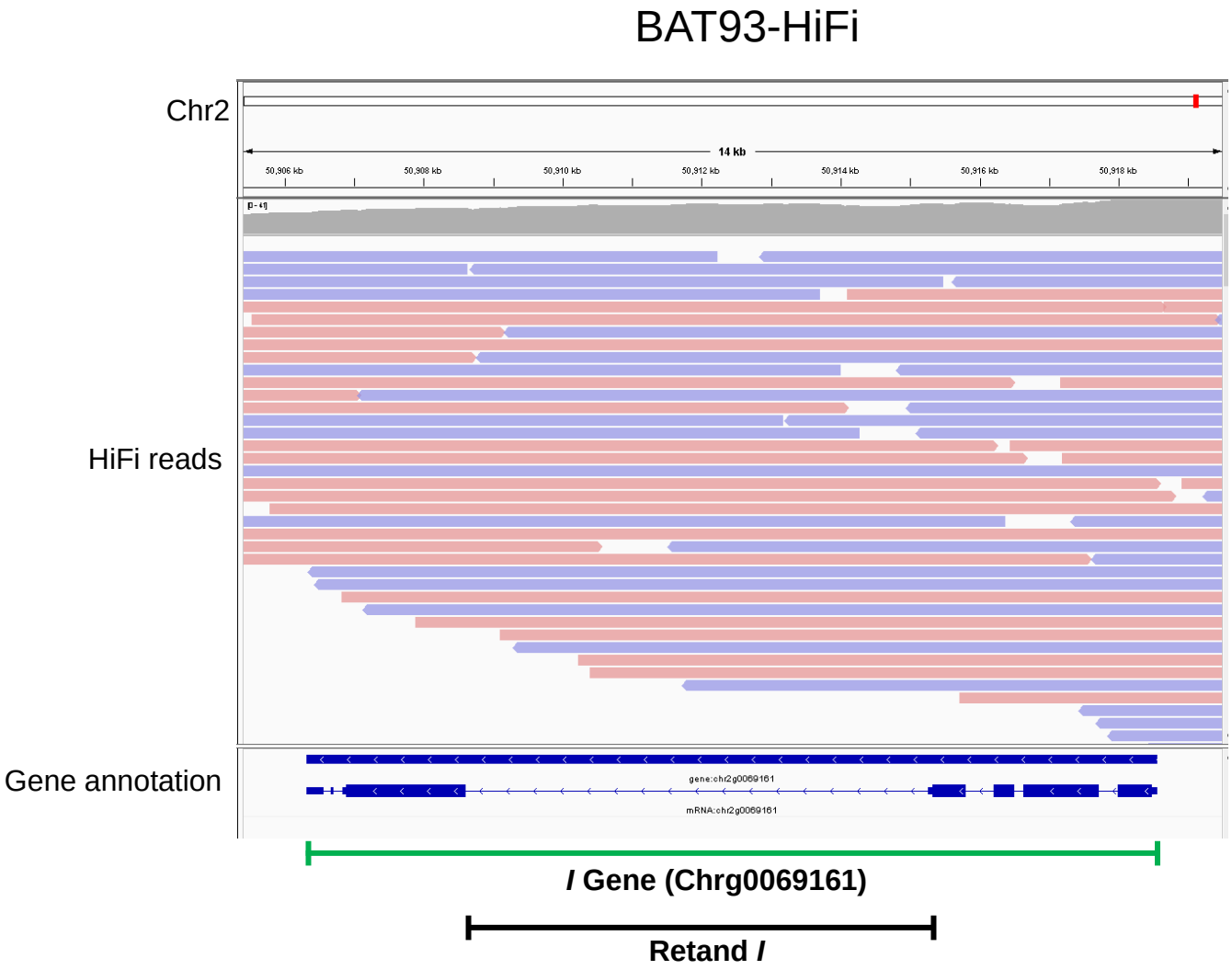

Supplementary Figure 6. Read coverage of the region containing gene 2 in BAT93-HiFi, visualized on IGV

a

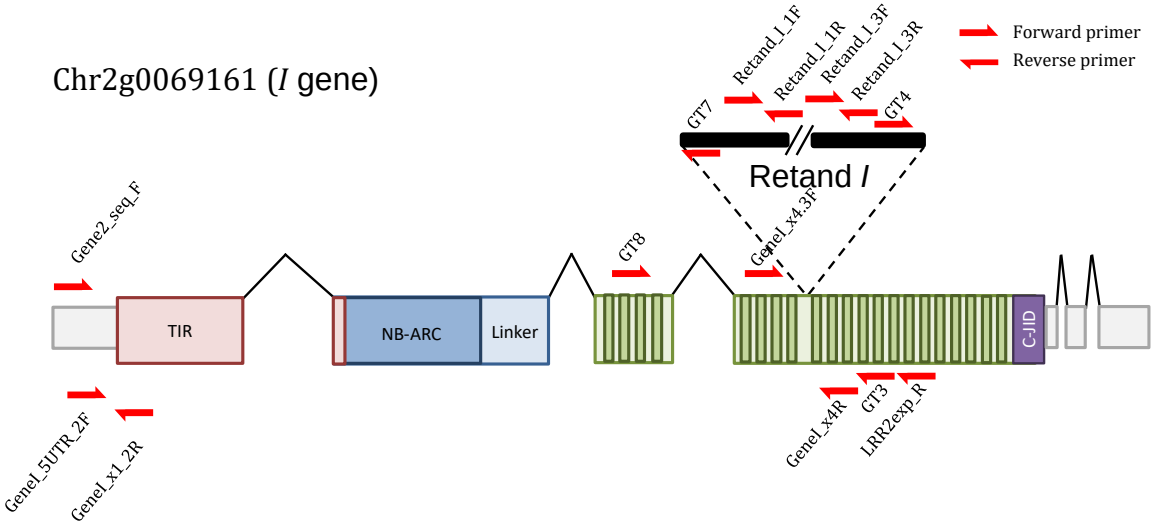

b

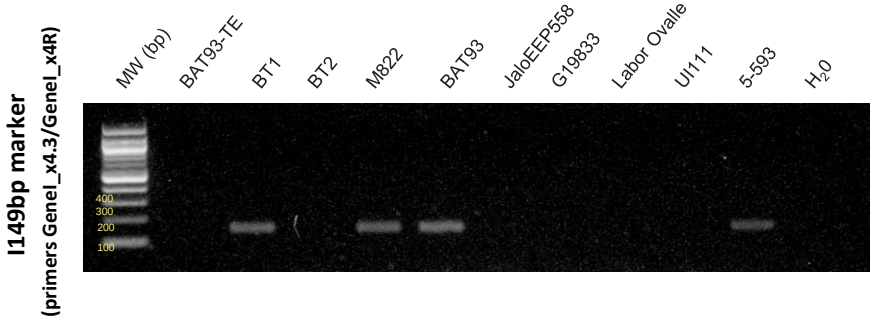

Supplementary Figure 7. Schematic representation of the *I* gene in BAT93 showing the position of the primers used in this study and the "I149pb" PCR-based marker specific of the *I* gene

a, Schematic representation of the *I* gene in BAT93-TE. The position of the primers used for transcriptional analysis and genotyping of the *I* gene and Retand *I* are indicated with red arrows. **b**, PCR-based marker specific of the *I* gene, referred to as "I149bp" using primers GeneI_x4.3F / GeneI_x4R. Whereas amplification of a 149 bp product is detected in the BAT93 and in the EMS BAT93-M822 mutant, no amplicon is detected in the mutant BAT93-TE due to the TE insertion, testifying that this marker is specific of the *I* gene and doesn't amplify any of the remaining BAT93 31 TNL. As expected, *I* gene is also detected in 5-593 and BT1 (Black Turtle1) (corresponding to *II* genotypes), whereas it is absent in BT2 (Black Turtle 2), JaloEEP558, G19833, Labor Ovalle and UI111 (corresponding to *ii* genotypes).

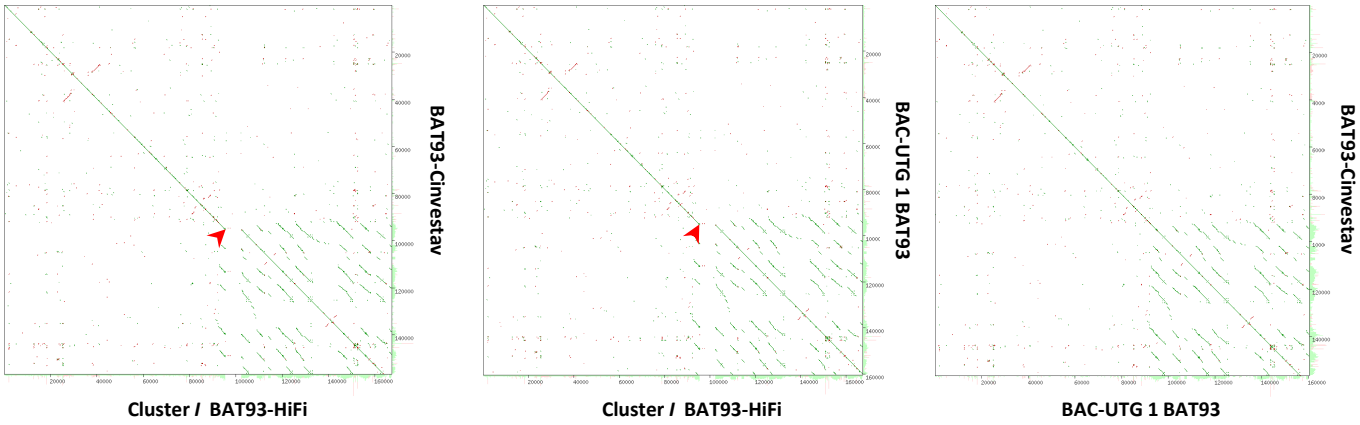

Supplementary Figure 8. Dot plot-based synteny comparison of the *I* cluster region in different sequences of BAT93

Nucleotide sequences BAT93-HiFi, BAT93-Cinvestav assemblies and the BAC sequence UTG1 corresponding to the *I* cluster were extracted and compared by dot plot. Red arrowhead shows the TE insertion site present only in the BAT93-HiFi assembly.

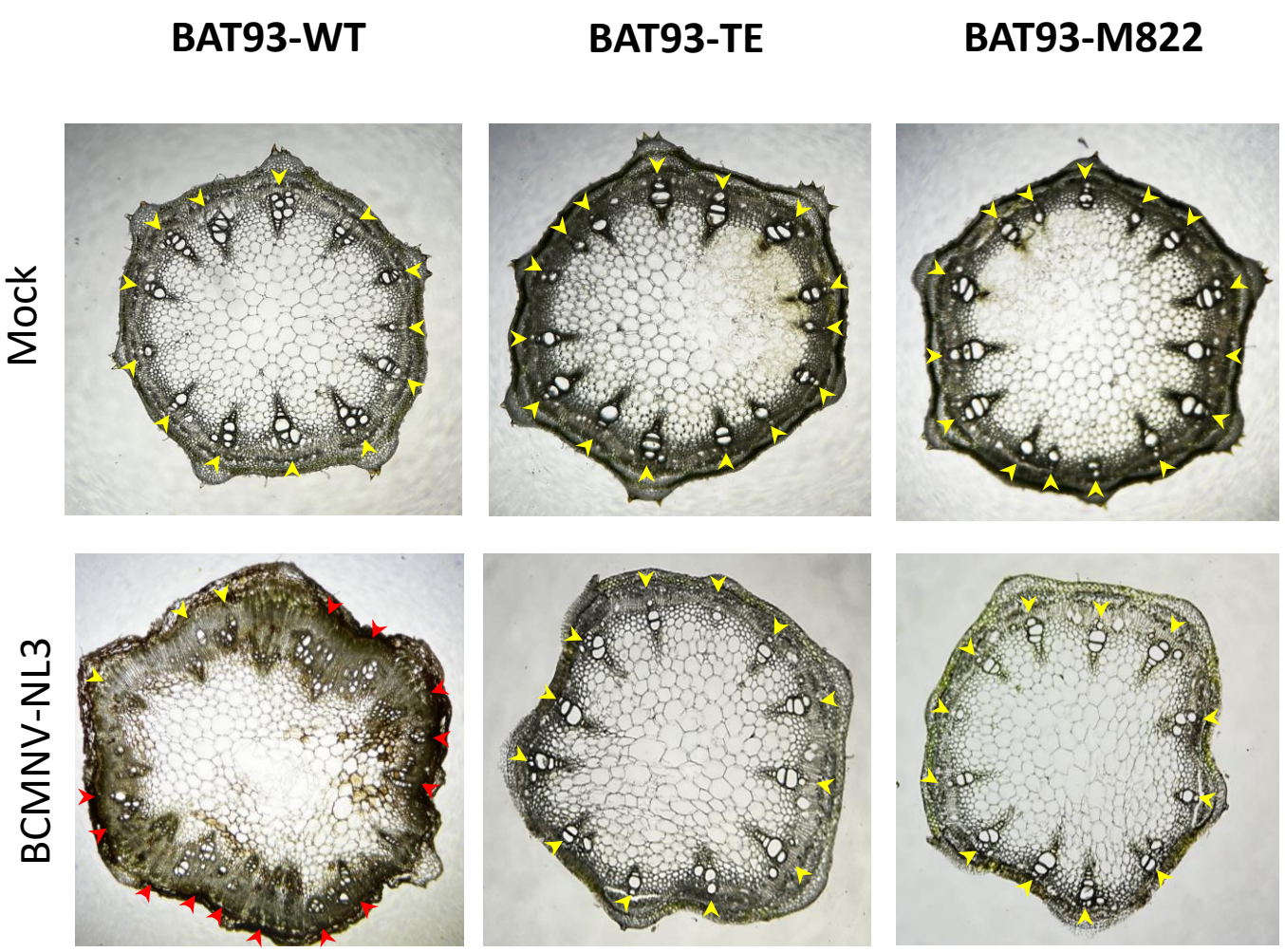

Supplementary Figure 9. Transversal stem cut from BAT93-WT and mutant plants infected with BCMNV-NL3 at 17 days post-inoculation

Transversal cuts were performed in the stem portion below the primary leaves by using vibratome steel blades. Yellow and red arrowheads indicate healthy and necrotic phloem tissues, respectively.

BAT93-M822

BAT93-TE

BAT93-WT

BCMV-US-6

Supplementary Figure 10. Phenotypes of infection with BCMV-US-6 in BAT93-WT and mutants

Observed phenotypes on complete plants from BAT93-WT and mutants at 21 days post-inoculation with BCMV strain US-6. Whereas no phenotype is visible on systemic leaves from BAT93-WT after BCMV infection, BAT93-TE and BAT93-M822 both present mosaic and crinkling symptoms on the trifoliate systemic leaves at 21 days post-inoculation with BCMNV strain US-6.

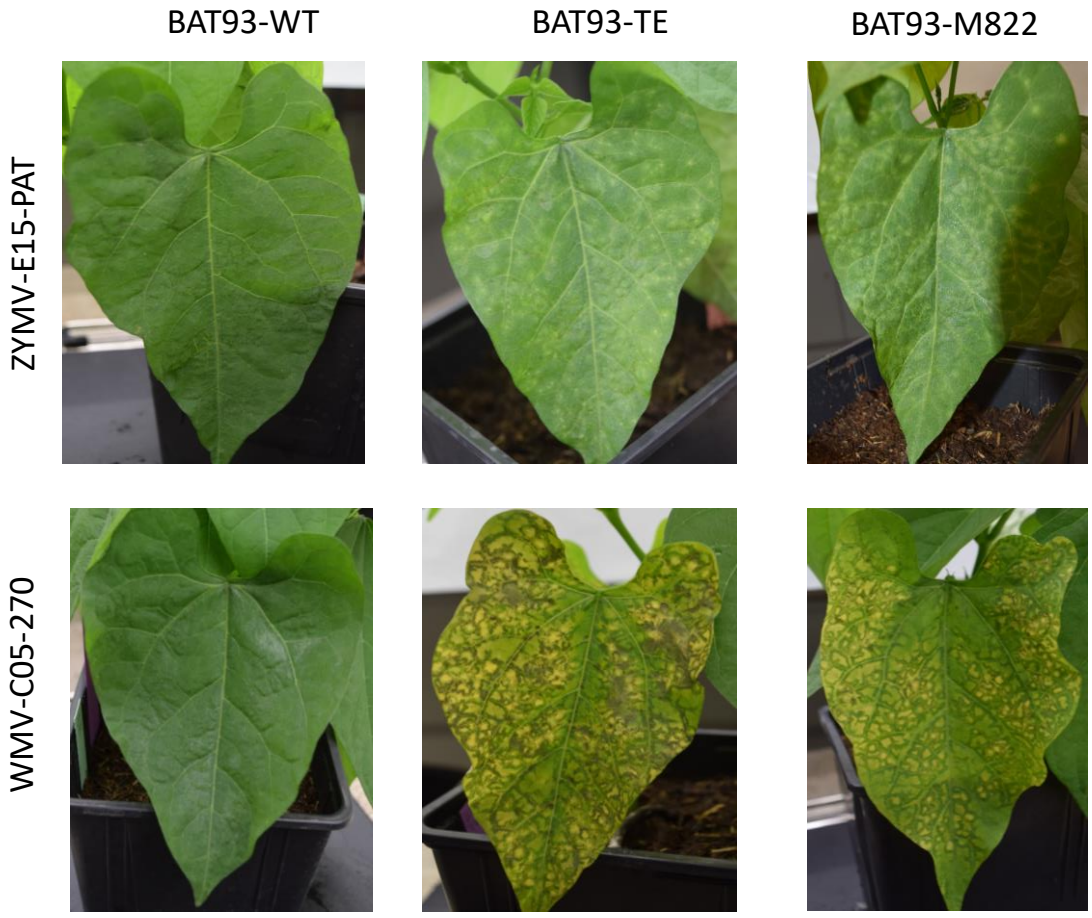

Supplementary Figure 11. Infection of BAT93 wild-type (WT) and BAT93 mutants (BAT93-TE and BAT93-M822) by ZYMV-E15-PAT and WMV-C05-270

Primary leaves of common bean BAT93-WT, BAT93-TE and BAT93-M822, three weeks after mechanical inoculation with ZYMV-E15-PAT (top) and WMV-C05-270 (bottom). Inoculated leaves of BAT93 presented no symptoms (extreme resistance) after inoculation with ZYMV-E15-PAT or WMV-C05-270. On the contrary, both *I* mutants (BAT93-TE and BAT93-M822) presented either mosaic symptoms (ZYMV-E15-PAT) or chloronecrotic lesions (WMV-C05-270) on the inoculated leaves. The upper uninoculated leaves of all plants were all asymptomatic for ZYMV; for WMV, in the second assay, chloronecrotic areas were observed in the first uninoculated trifoliate leaves of BAT93-TE and BAT93-M822 (data not shown).

a

Retand *I* LTRs alignment

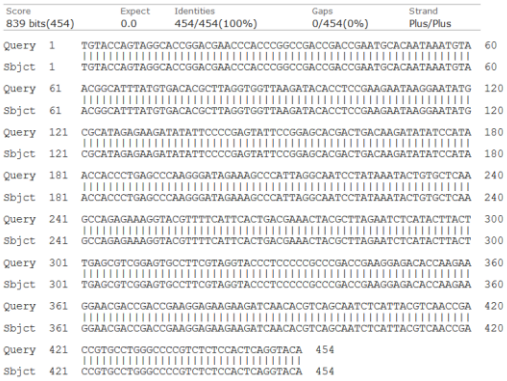

b

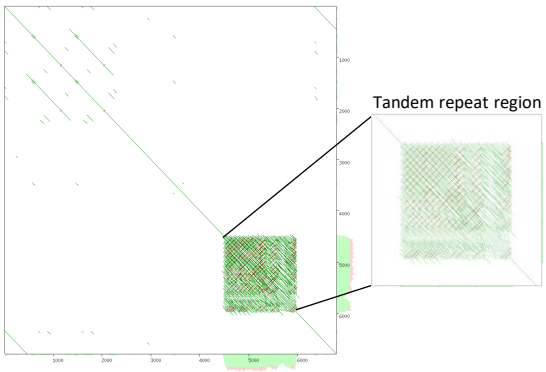

c

Supplementary Figure 12. Characterization of Retand *I* repetitions

a, Sequence alignment of LTRs in the Retand *I* retrotransposon. **b**, Dot plot representation of the nucleotide sequence of Retand *I*. **c**, Multiple alignment of 20 identified monomers of the tandem repeat array. Gaps in the alignment are indicated by dashes; nucleotides that differ from prevalent bases of the consensus are highlighted in yellow and sub-repeats of tandem repeat monomers are indicated on the bottom.

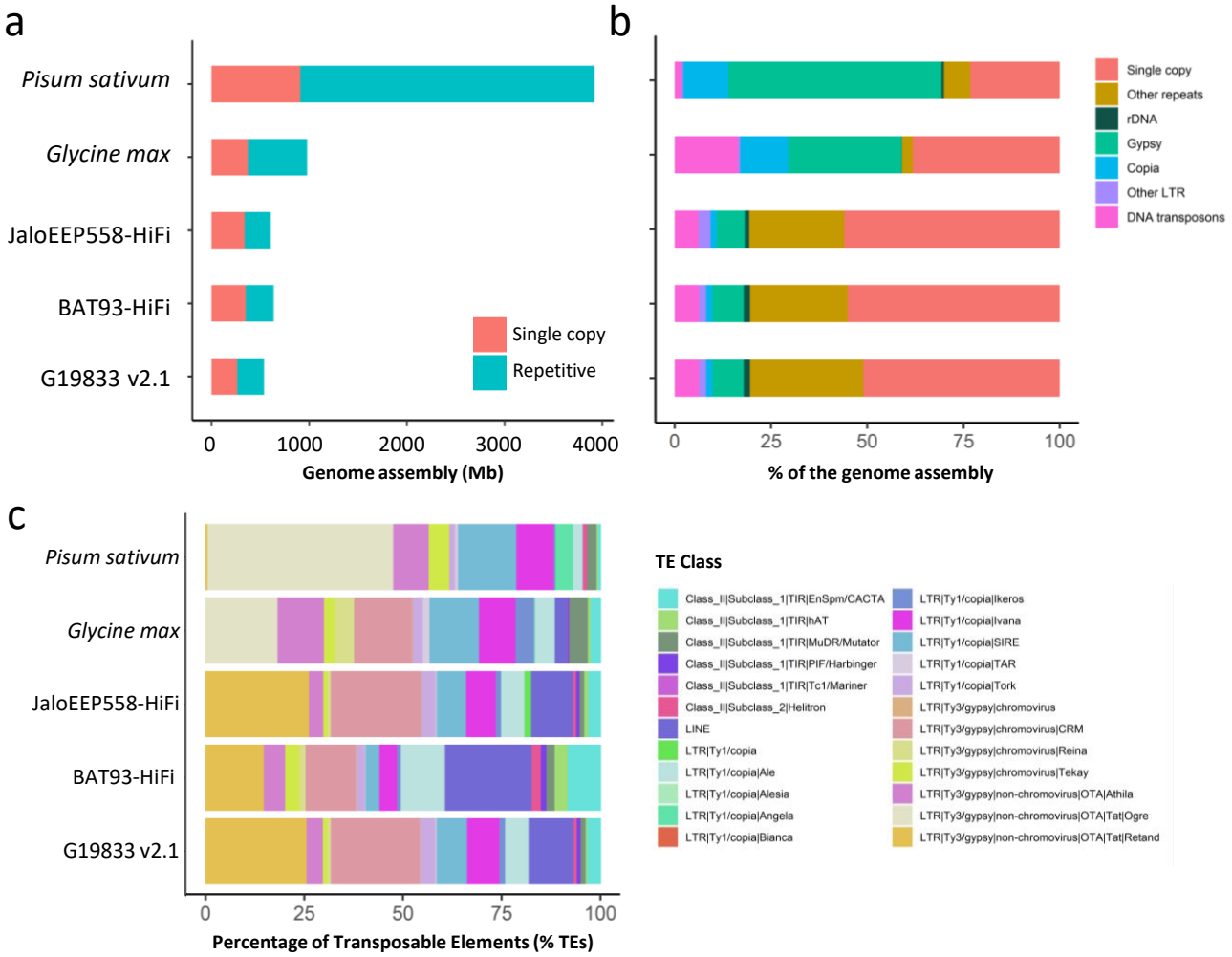

Supplementary Figure 13. Repetitive sequence composition in *P. vulgaris* genome assemblies compared with other legume genomes. a, Single copy and repeated sequence content in different genome assemblies of legume species. **b,** Proportion of single copy and repeated sequences for the different classes of repeats. **c,** Summary of the *P. vulgaris*, soybean and pea transposable elements composition by family.

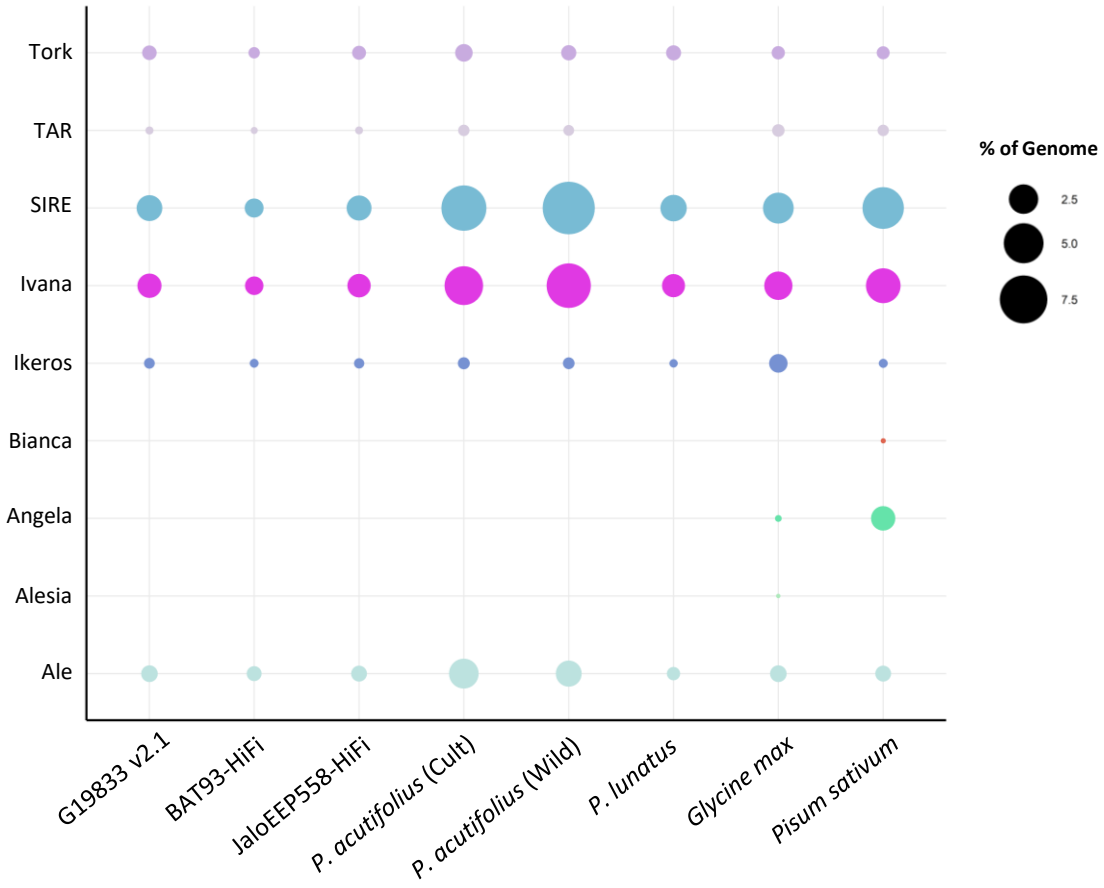

Supplementary Figure 14. Percentage of the genome occupied by the different Copia TE families in different legume genome assemblies

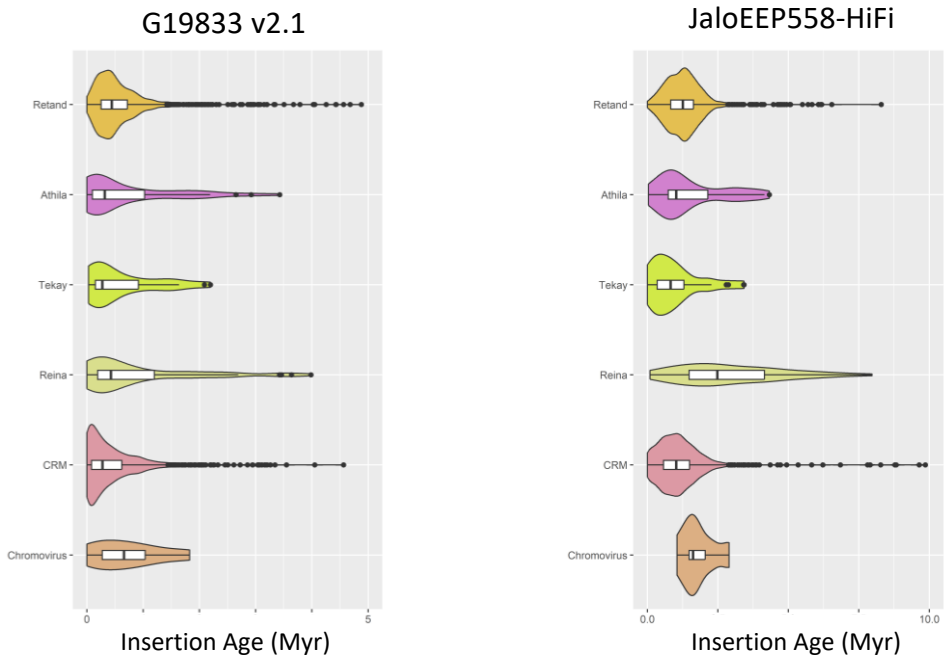

Supplementary Figure 15. Age distribution of full-length element long terminal repeat-retrotransposon (LTR-RT) Gypsy families in the G19833 v2.1 and JaloEEP558-HiFi genome assemblies

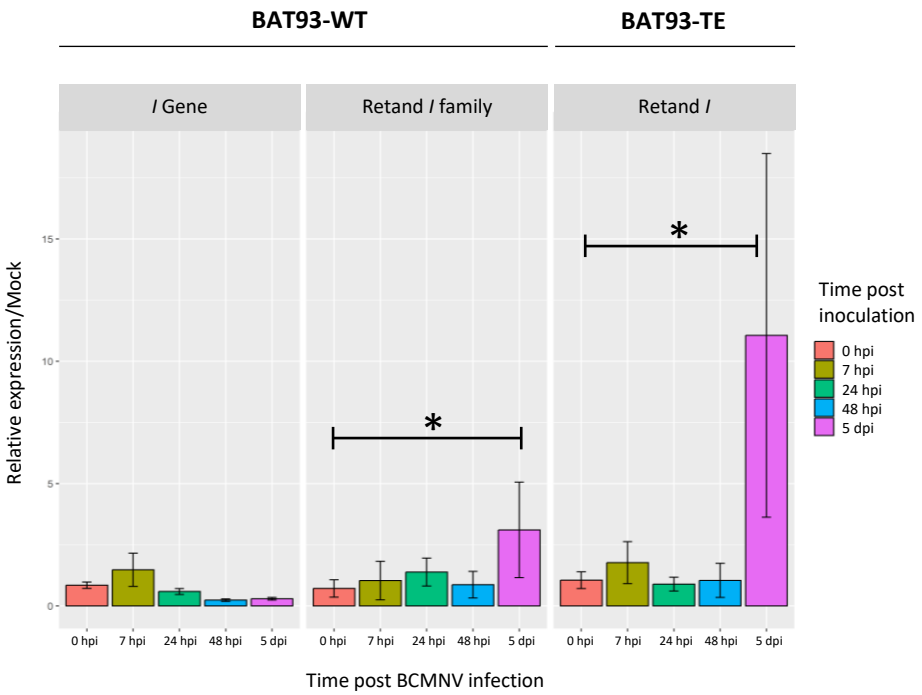

Supplementary Figure 16. Expression of the *I* gene and Retand elements in response to biotic stress (BCMNV infection)

Relative expression level of *I* gene, Retand *I* family, and the Retand *I* in BAT93-WT and BAT93-TE at different times after BCMNV infection. Data are mean ± s.d. (n = 3 independent samples, three independent experiments). Comparison between treatments was performed using the non-parametric Wilcoxon-Mann-Whitney U-test. Asterisks indicate the level of significance: * $p < 0.05$, ** $p < 0.01$ and *** $p < 0.001$.

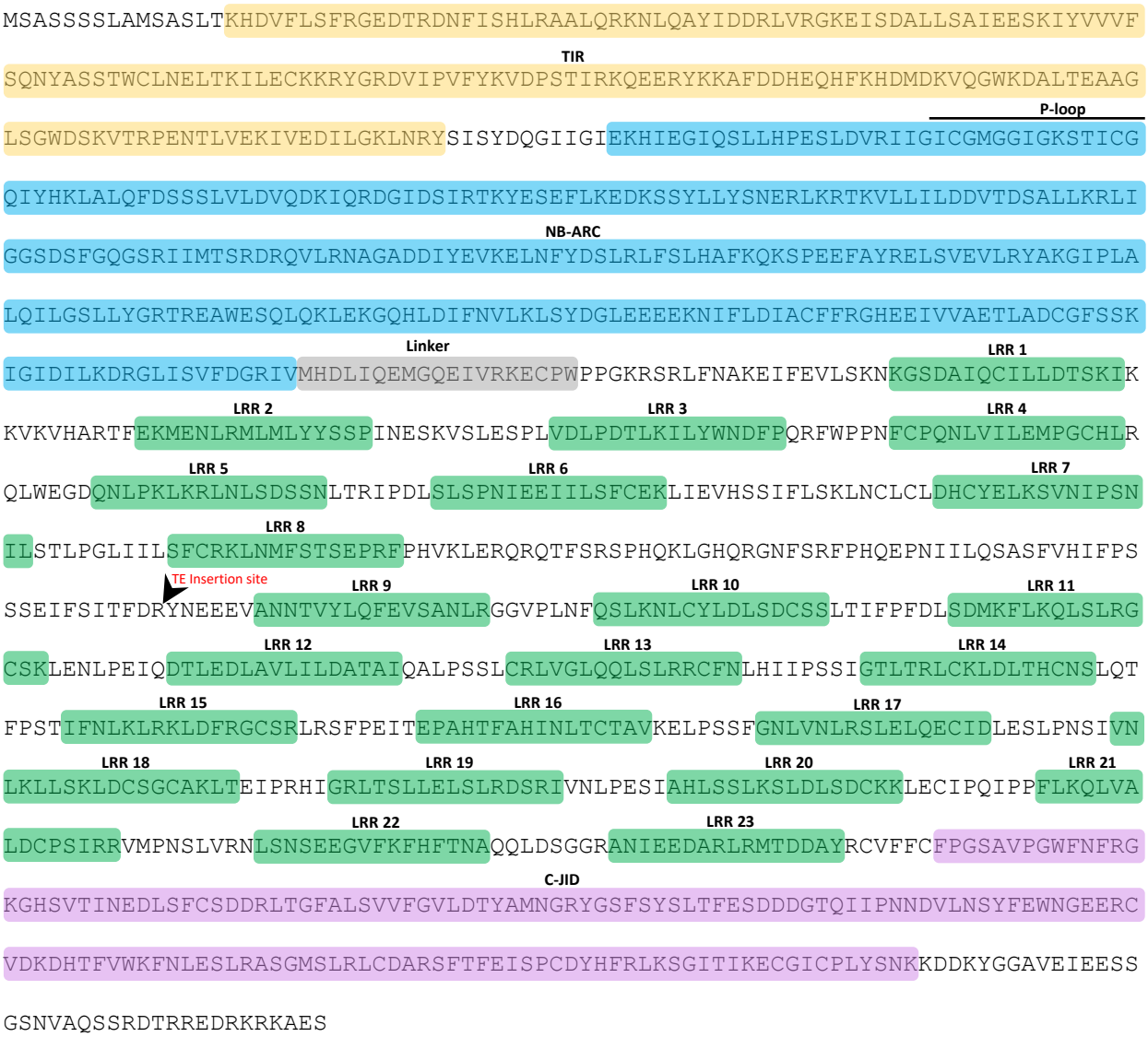

Supplementary Figure 17. Sequence analysis of the protein encoded by *I* gene in BAT93-WT
Each protein domain is shaded in different colors: TIR domain (yellow), NB-ARC domain (blue), Linker domain (grey), LRR domain (green) and C-JID domain (purple). Black arrowhead indicates the TE insertion site in the corresponding DNA sequence in the BAT93-HiFi assembly.

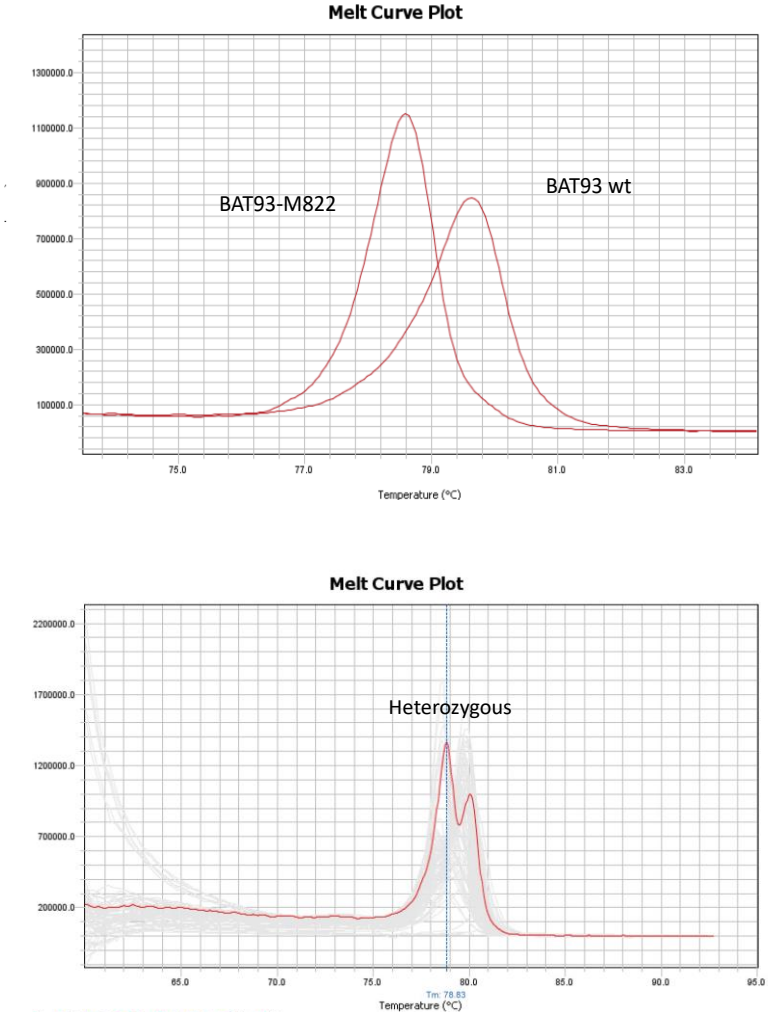

Supplementary Figure 18. Melting curve analysis of the splice acceptor variant identified in the *I* candidate gene from BAT93-M822 mutant, genotyped by the Tm-shift method